Solid Earth Discuss., doi:10.5194/se-2016-2, 2016
Manuscript under review for journal Solid Earth
Published: 18 January 2016

Seismic structure beneath the Gulf of Aqaba and adjacent areas based on the tomographic inversion of regional earthquake data

Sami El Khrepy[1,2] (k_sami11@yahoo.com, , corresponding author),

Ivan Koulakov[3,4] (ivan.science@gmail.com , corresponding author),

Nassir Al-Arifi[1] (nalarifi@ksu.edu.sa),

Alexey Petrunin[5,6,7] (alexei@gfz-potsdam.de)

1. King Saud University, Riyadh, Saudi Arabia**,** P.O. Box 2455, Riyadh 11451, Saudi Arabia.
2. National Research Institute of Astronomy and Geophysics, Seismology department, NRIAG, 11421, Helwan, Egypt
3. Trofimuk Institute of Petroleum Geology and Geophysics SB RAS, Prospekt Koptyuga, 630090, Novosibirsk, Russian Federation
4. Novosibirsk State University, Novosibirsk, Russia
5. Goethe-University, 60323 Frankfurt M, Germany
6. GeoForschungsZentrum-Potsdam, Telegrafenberg, 14473, Potsdam, Germany
7. Schmidt Institute of Physics of the Earth, B. Gruzinskaya 10, Moscow, Russia

Submitted to Solid Earth

December, 2015

Novosibirsk, Riyadh, Potsdam

Solid Earth Discuss., doi:10.5194/se-2016-2, 2016
Manuscript under review for journal Solid Earth
Published: 18 January 2016

Abstract

The Gulf of Aqaba is an elongated basin (~180 x 20 km) with depths reaching 1850 m. It represents the southern segment of the Dead Sea Transform (DST), which is one of the largest transform fault zones in the world. The opening of Gulf of Aqaba is thought to have originated from the relative displacement of the African and Arabian Plates. According to historical and recent earthquake records, it is seismically active. In this study, we present the first 3D model of seismic P and S velocities beneath the Gulf of Aqaba area based on the results of passive travel time tomography. The tomographic inversion was performed based on travel time data from ~9000 regional earthquakes provided by the Egyptian National Seismological Network (ENSN) and the International Seismological Center (ISC). The inversion results are generally consistent for P- and S-velocity patterns at all depths. At all depth intervals in the Red Sea, we observed strong high-velocity anomalies with abrupt limits that coincide with the coastal lines. This finding suggests that the oceanic nature of the crust in the northern Red Sea does not support the concept of gradual stretching of the continental crust. According to our results, in the middle and lower crust, the seismic anomalies seem to delineate a sinistral shift (~100 km) in the opposite flanks of the fault zone that is consistent with other estimates of the left-lateral displacement in the southern part of the DST. However, no displacement structures are visible in the upper-most lithospheric mantle.

Key words: Seismic tomography, Gulf of Aqaba, Dead Sea Transform, Northern Red Sea

Introduction

Tectonic activity in the Gulf of Aqaba region is responsible for high levels of seismicity, which represent a significant hazard for the local population. In 1993 and 1995, two strong earthquake sequences with magnitudes reaching Mb=5.8 and Mb=6.7 (main shocks), occurred beneath the Aqaba basin (Abdel Fattah et al., 1997; Hofstetter, 2003). Sharp bathymetry features

Solid Earth Discuss., doi:10.5194/se-2016-2, 2016
Manuscript under review for journal Solid Earth
Published: 18 January 2016

of the Gulf Aqaba floor and the presence of deep-sea segments reaching depths of 1850 m (Figure 1b) provide evidence for ongoing active tectonic processes (Ben-Avraham et al., 1979; Ehrhardt et al., 2005; Makovsky et al., 2008). It appears that in some parts of the Gulf of Aqaba, the sedimentation rate cannot compensate for the rapid subsidence of the sea floor (Ten Brink et al., 1993). This differs from the Gulf of Suez, which is located on the other side of the Sinai Peninsula; many considered it to be a zone of ongoing crustal extension (McClusky et al., 2003; Mahmoud et al., 2005), and it is nearly fully covered by young sediments (Gaullier et al., 1988; Cochran and Martinez, 1988).

The Gulf of Aqaba represents a transition zone from the spreading ridge in the Red Sea to the strike slip Dead Sea Transform Fault (DST) (Ben-Avraham et al., 1979). A very similar transition occurs in the Gulf of California at the southern edge of the San Andreas Fault. Many researchers (Joffe and Garfunkel, 1987; Ehrhardt et al., 2005) accept that the opening of the Gulf of Aqaba occurred simultaneously with the initiation of the Dead Sea Transform Fault (DST) 20-15 Ma ago. This fault is one of the largest faults in the world and can be traced for more than 1000 km from the Red Sea to the westernmost end of the Zagros collision zone in eastern Turkey. It cuts the continental crust along the Eastern margin of the Mediterranean Sea. GPS observations provide rates of the present left lateral displacement along the DST fault in the range of 3.5-4 mm per year (Gomez et al., 2007; Wdowinski et al., 2004). Geological observations provide evidence for faster rates, ranging from 5 to 10 mm per year, of long-term displacements starting from the initiation of the DST 20-15 Ma ago (Garfunkel, 1981; Chu and Gordon, 1998). Based on geological observations, the total displacement in a segment of the DST between the Gulf of Aqaba and the Dead Sea was estimated to be 105 km (Freund et al., 1968; Bartov et al., 1980; Garfunkel et al., 1981). To the north of the Dead Sea, the displacement is considerably less (Garfunkel, 1981).

The initiation of the DST was due to the relative displacements of the African and Arabian plates (Figure 1a). In the no-net-rotation reference frame, the African and Arabian Plates

Solid Earth Discuss., doi:10.5194/se-2016-2, 2016
Manuscript under review for journal Solid Earth
Published: 18 January 2016

both move northward, but their displacement vectors differ slightly in their lengths and orientations (Smith et al., 1994; McClusky et al., 2003) that leads to the divergence of the African and Arabian Plates in the area of the Red Sea and results in the spreading of this ocean-type basin. In the area of the Dead Sea and to the north, the displacement vectors of these plates are nearly parallel; however, the Arabian Plate moves faster, resulting in conditions for transform faulting.

Although the link between the opening of the Aqaba basin and the initiation of DST displacement is generally accepted, the details of this process are still debated. Most scholars associate the origin of deep linear depressions along the DST, such as the Gulf of Aqaba and the Dead Sea, with the pull-apart mechanism (Mann et al., 1983; Petrunin and Sobolev, 2008; Makovsky et al., 2008; Hartman et al., 2014). Lateral displacements along a non-straight fault line should lead to the origin of compression and extension zones at the vicinity of the fault. Many studies have used both numerical modeling (Petrunin and Sobolev, 2008; Petrunin et al., 2012) and geological evidence (Ehrhardt et al., 2005) to demonstrate the possibility of such a scenario.

Alternatively, the origin of the present depressions along the DST can be explained by the relative transform-normal extension (Ben-Avraham and Zoback, 1992; Smit et al, 2010) due to relocation of pole of rotation for the DST at about 5 Ma (Garfunkel, 1981). The left plot in Figure 2 depicts a possible structure before the initiation of DST. In this reconstruction, the coastal structures form continuous trends in NW-SE directions indicated with red lines. The present configuration, shown in the right plot, is obtained by a left-lateral displacement of the Arabian Plate to ~100 km with a simultaneous counter-clockwise rotation to 2.7°. The total displacement is generally consistent with estimates made by other researchers, based on the similarity of geological strata (Freund et al., 1968). In this plot, red lines along the DST mark the location of the initial fault in the opposite flanks. Between these lines, there is an extension zone that corresponds to the Gulf of Aqaba and the Dead Sea. This reconstruction demonstrates the origin of the Aqaba basin resulting from simultaneous relative rotation of the Arabian Plate and an offset along the DST. For the Dead Sea, we have defined a step-shaped feature on the fault that facilitates the extension due to the pull-apart mechanism.

A further understanding of the mechanisms of tectonic processes in this area requires robust information on the deep crustal and mantle structures. There is a large difference in the studies that have examined different segments of the DST. The most comprehensive studies have been performed in the area of the Dead Sea (DESERT Group, 2004; Weber et al., 2009). Several passive and active seismic experiments of different scales, receiver functions, and magneto-telluric studies have provided information on the crustal and upper mantle structures (Mechie et al., 2005; Ritter et al., 2003; Mohsen et al., 2006).

Unfortunately, most of these comprehensive studies cover the areas to the north of the Aqaba basin and do not provide much information on the structures beneath the Gulf of Aqaba. Between the 1960s and 1980s, some reflection and refraction seismic studies used active sources to explore the detailed crustal structure beneath Gulf of Aqaba, although primarily in the upper part (Ben-Avraham et al., 1979, Ginsburg et al., 1981, Ben-Avraham, 1985, Makovsky et al., 2008, Hartman et al., 2014). Seismic refraction data revealed a gradual southward decrease of the Moho depth from ~35 km at the northern edge of the Gulf of Aqaba to ~27 km in the southern part. These results helped identify some of the fault structures that can be used to explain the mechanisms of the opening of the Aqaba basin (Figure 1b).

Several regional studies were performed for large areas of Asia and Africa that included the Gulf of Aqaba. Large-scale surface wave tomography studies by Park et al., (2008) and Chang and van der Lee, (2011) did not reveal any particular features related to the Aqaba basin. According to the models of the crustal structure and Moho depth for the entire Eastern Mediterranean region by Koulakov and Sobolev (2006) and Mechie et al. (2013), the crust to the north of the Gulf of Aqaba is locally thicker than that of other areas. A recently derived seismic model for the upper mantle beneath the Arabian region (Koulakov et al., 2015) gives fair resolution for the Sinai, Aqaba, and Dead Sea regions; however, it does not provide any information for structures above a 100 km depth.

Between detailed seismic surveys in the Aqaba region and large-scale regional tomographic models, there is a gap in studies of the crust and uppermost mantle beneath the Gulf of Aqaba and surrounding areas. Although there is active seismicity in this region and a fair amount of seismic stations on both sides of the Gulf of Aqaba, no detailed earthquake tomography was performed. Here, we present the first tomographic model based on a large dataset, which was provided by the Egyptian National Seismological Network (ENSN). The new 3D models of P- and S-velocities give a new look to the structure beneath the Gulf of Aqaba and surrounding regions and enhance our knowledge of the deep mechanisms driving the geodynamic processes in this region.

Data and Algorithm

In this study, we used the arrival times of P and S seismic waves from seismicity occurring beneath the Gulf of Aqaba and surrounding regions. The dataset was mostly extracted from the Catalogues of the Egyptian National Seismological Network (ENSN) and was complemented by data from the International Seismological Center (ISC) catalogues to enlarge the study area and improve data sampling. The collected arrival time data from different catalogues merged into one catalogue for the same events list. When merging events presented in both catalogues, higher priority was given to the data of the ENSN. The data used in this study are part of a dataset that covers a much larger area than presented in the resulting maps. This helped us avoid some of the edge effects that occurred when stations and/or events were located close to the limits of the processed area. The data for this study were recorded by approximately 300 seismic stations in Egypt and surrounding countries; of these stations, only 53 were located in the study region (Figure 3). The same dataset was used in a recent study by Khrepy et al. (2016) providing crustal and uppermost seismic structures beneath the Gulf of Suez.

In total, we used more than 9000 events over all of Egypt, of which approximately 3000 events corresponded to the Aqaba region and northern Red Sea (Figure 3). To select the data for tomography, we used a criterion of a minimum of 6 picks with any phases (P or S) per event. In total, we selected ~65,000 P and ~17,000 S picks, with an average of 9 picks per event. The relatively small ratio is due to a sparse distribution of stations and mostly low magnitudes of events. To remove outliers from the data, we selected the picks with absolute residuals of less than 1.5 and 2 seconds for the P and S data, respectively, that corresponded to the stage of source location in the starting 1D velocity model.

The tomographic inversion was performed using LOTOS code (Koulakov, 2009), expanded for the case of large areas. This algorithm accounts for the sphericity of the Earth when computing the travel times of seismic rays. This code has been described in many previous tomography studies; thus, we only briefly present the major steps and features. The workflow begins with a preliminary calculation of source locations based on the grid search method. For faster calculations, we approximated the model travel times by using a set of tabulated values derived at a preliminary stage. Then, the locations of sources were recomputed using the 3D ray-tracing algorithm based on the “bending method” (Um and Thurber, 1987). The 3D velocity distribution was parameterized using nodes that were distributed in the study area according to the density of rays. The minimum grid spacing was defined as 10 km in the horizontal direction and 3 km in the vertical direction. The distribution of the parameterization nodes, together with the ray paths, corresponding to the depth sections of 10 and 30 km are presented in Figure 4. To reduce grid dependency, we performed the inversions for four differently oriented grids with basic orientations of 0°, 22°, 45° and 67° and then averaged the results. The inversion was performed simultaneously for 3D P and S anomalies, source corrections (4 parameters for each source), and station corrections. The velocity solution was damped by a smoothing matrix, which minimizes the velocity gradients between all neighboring parameterization nodes. The inversion was performed using the LSQR algorithm (Page and Saunders, 1982; Nolet, 1987). The steps of

Solid Earth Discuss., doi:10.5194/se-2016-2, 2016
Manuscript under review for journal Solid Earth
Published: 18 January 2016

source locations in the derived 3D models, the calculation of the first derivative matrix, and the inversion were iterated five times (a compromise between the computing time and accuracy of the solution). The values of free parameters (e.g., weights for smoothing, station and source corrections) were determined based on the results of synthetic modeling. Values of the main parameters used for calculation of the main model are given in Table 1.

Table 1. Values of some parameters used to calculate the main tomographic model

Parameter description	**Value**
Grid spacing, horizontal	10 km
Minimum grid spacing, vertical	3 km
Minimum number of picks per event	6
Maximum residual deviation, for P and S	1.5 and 2 s
Number of the LSQR iterations	100
Smoothing for the P velocity	1.5
Smoothing for the S velocity	3
Amplitude damping, P and S	0 and 0
Station corrections, P and S	0.1 and 0.3
Weight for the source coordinate correction	5
Weight for the source origin time correction	5

The data analysis began with finding an optimal starting velocity model. We used a fairly simple approximation, implying a 1D distribution of P-velocity and a constant value of the Vp/Vs ratio. The P-velocity was defined in several depth levels; between these depths, the velocity was linearly interpolated. The optimal model was determined using the trial method. The initial location of sources (i.e., grid search with tabulated travel times) was performed in many different models using different P-velocities and Vp/Vs ratios. The best model is the one that provides the minimum number of rejected outliers and minimum values of average residual

Solid Earth Discuss., doi:10.5194/se-2016-2, 2016
Manuscript under review for journal Solid Earth
Published: 18 January 2016

Solid Earth Discussions Open Access EGU

deviations. We performed the optimization for the entire dataset of the Egyptian networks and obtained an optimal Vp/Vs value of 1.74. The distribution of the optimal P-velocity is presented in Table 2.

Table 2. The optimal 1D P-velocity distribution used as a reference model for the tomographic inversion

Depth, km	P-velocity, km/s
-3	4.9
10	6.0
20	6.7
30	7.5
50	8.0
100	8.2

Results

Before discussing the main velocity models, we present the results of synthetic tests assessing the horizontal and vertical resolution. Synthetic data were computed using the same ray configuration as the observed data catalogue used to calculate the main tomography model. The synthetic travel times were calculated using the algorithm for 3D ray-tracing based on the bending method. Random noise with a magnitude of 0.15 s was added to the synthetic travel times. Before starting the reconstruction, we perturbed the locations of events and origin times so their true values remained unknown. The reconstruction procedure included all of the steps provided by the LOTOS code, including the preliminary locations of sources in the starting 1D model. This step strongly biases the synthetic residuals and leads to a trade-off between source and velocity parameters, similar to the processing of observed data. The synthetic tests help derive the most optimal values for the inversion parameters and enable the highest quality reconstruction. These parameters were then used to perform the inversion of the observed data.

Solid Earth Discuss., doi:10.5194/se-2016-2, 2016
Manuscript under review for journal Solid Earth
Published: 18 January 2016

Solid Earth Discussions Open Access EGU

Here, we present results for two synthetic models. The first model (Figure 5) was used to assess the horizontal resolution. In this case, cells with positive and negative anomalies with an amplitude of ± 5% and a size of 50x50 km were defined without depth changes. The reconstruction of this model is presented at four depth levels. This model is generally well recovered in most parts of the study area. Some loss of resolution is observed for the S-model at the 40 km depth.

The second model (Figure 6) was aimed at estimating the vertical resolution. Due to the trade-off between source and velocity parameters, in most cases of earthquake tomography, the vertical resolution is lower than the horizontal resolution. In this test, we defined checkerboard anomalies along the same vertical sections, as was used for presenting the main results. Across the section, the thickness of anomalies was 40 km. The presented results were obtained from the reconstruction of three separate models. In two of these models, the anomalies were defined along single sections (1 and 3), and in one model, anomalies in both the 2nd and 4th sections were defined. Here, we show the results for the P-model; for the S-model, the resolution appeared to be similar. We see that in most sections, the change in the anomaly sign at 15 km depth is correctly recovered. The anomalies between 15 and 45 km are only recovered in the presence of deep earthquakes; alternatively, they are strongly smeared. Beneath the Gulf of Aqaba and surrounding areas, we can resolve the second boundary of change in the anomaly sign at 45 km. This test shows that the vertical resolution is strongly variable; this should be considered when interpreting the results.

Five iterations were performed for the inversion of observed data. During the inversions, the average absolute residuals were reduced from 0.232 to 0.173 seconds (25.5%) for the P-data and from 0.348 to 0.208 seconds (40.2%) for the S-data. The values of the final residuals are generally compatible with the picking accuracy estimates reported by the ENSN. The larger reduction for the S-data seems to be paradoxical, considering the lower quality of the S-picks. However, the S-data are more sensitive to velocity anomalies because the same percent value of an anomaly gives a larger S-residual compared with the P-residual. In addition, the amplitudes of the S-anomalies are usually stronger than those of the P-anomalies.

The inversion results for the P- and S-anomalies are presented in horizontal sections in Figure 7. For reference, in the section at the 10 km depth, we show the locations of the main faults. At the 20 and 30 km depths, we give reconstruction markers of the left-lateral displacement of DST introduced in Figure 2. Velocity anomalies are shown only in areas with a sufficient amount of data. Outside the resolved areas, the anomalies are shaded.

Absolute P and S velocities are shown at 30 km depth with four vertical sections (Figures 8 and 9). The contour lines in the vertical sections roughly represent deviations in the main interfaces. For example, Vp=7.3 km/s and Vs=4.3 km/s (violet layer) are the average values between the lower crust and uppermost mantle and may represent the Moho interface. Beneath the Red Sea, the crustal thickness is approximately 20 km. The largest crustal thickness observed was in the area of DST (northern part of Section 1) and beneath Saudi Arabia (NE part of Section 2), where the Moho depth reaches ~40 km. A relatively thin crust (25-30 km) is observed beneath the middle part of Sinai (NW part of section 3 and SW part of Section 4). The maps of absolute velocities at 30 km show different areas corresponding to mantle velocities beneath the Red Sea and crustal velocities in most of surrounding areas. A more detailed description of these models and interpretation is given in the next section.

An informal argument for the robustness of the computed tomography models is the clear correlation of the main P- and S-velocity anomalies. Although P- and S-velocities should not necessarily fit each other, in practice, the main geological structures behave similarly in both cases, especially on a large scale. Thus, the correspondence of the P- and S-velocities might serve as a “first look” verification of the results.

Discussion

Solid Earth Discuss., doi:10.5194/se-2016-2, 2016
Manuscript under review for journal Solid Earth
Published: 18 January 2016

The resulting 3D models of the P- and S-velocity anomalies are presented in horizontal sections in Figure 7; the absolute velocities are shown in Figures 8 and 9. These velocity distributions can be compared with previous results of various scales based on different methods. For example, in the regional tomography model by Chang and van der Lee (2011), the study area is entirely located within one large low-velocity pattern. The other regional tomography models mentioned in the introduction are also too rough to identify the details observed in the present model. Some similarities are observed with seismic velocity anomalies for the Aqaba region in the model by Koulakov and Sobolev (2006), which was based on the data from the ISC catalogues, especially for the distributions of the S anomalies. However, that area was on the margin of the model and thus had lower data density and poorer resolution. For the upper mantle, the P-velocity model is similar to a recent tomography model of the entire Arabian region by Koulakov et al. (2015), in which the southern part of the Gulf of Aqaba corresponds to the higher-velocity anomaly at 100 and 200 km depths. Meanwhile, the large area corresponding to the Dead Sea and surroundings coincides with the lower-velocity anomaly.

The main feature, which is clearly observable in both P- and S-velocity models, is a strong high-velocity anomaly that corresponds to the Red Sea. At the 30 km depth, the high velocity in the Red Sea may be related to a significantly thinner crust. In offshore areas, this depth corresponds to the mantle, whereas in continental areas, this is still the lower crust. The high-velocity anomalies in the upper sections may support the notion for the prevalence of mafic rocks with higher velocities compared with felsic rocks typical for the upper continental crust in surrounding areas. This fact may renew debates regarding the nature of the crust in the northern Red Sea. According to a concept proposed by some authors (e.g., Cochran and Martinez, 1988) based on absence of clear signature of spreading ridges and linear magnetic anomalies (e.g. McKenzie et al., 1970), the crust in the northern part of the Red Sea was formed due to gradual stretching and, as a result, has both felsic and mafic components. However, more recent studies

(Cochran, 2005; Cochran and Karner, 2007) report clear axial depression of bathymetry and aligned magnetic anomalies as well as a chain of dykes that are more typical for rifting processes. In our study, we see that the high-velocity anomaly in the Red Sea has very sharp bounds coinciding with the coastline; this presumes an abrupt difference in crustal properties between the on- and off-shore areas at all depth intervals. This would mean that the upper felsic crust is almost absent at this area. This would be not possible in the case of gradual stretching of the continental crust. We propose that such slow spreading might be due to a dispersed system of dykes covering large areas of the sea bottom. However, to prove this hypothesis, additional studies are required.

At the 10 km depth, in addition to the large high-velocity anomaly beneath the Red Sea, the structure of the P- and S-anomalies are unexpectedly inconsistent with the distribution of the main geologic units. Neither the location of the Gulf of Aqaba nor the distributions of the main faults can be unambiguously associated with seismic anomalies. The seismic patterns in the Aqaba area look patchy and non-structured. However, after shifting the eastern flank with respect to the western one according to our back-reconstruction (Figure 2), the structures become more consistent (Figure 10). For example, the negative seismic anomalies at the 10 km depth seem to form two continuously curved zones, which are highlighted with violet lines that appear to be nearly parallel. These anomalies may represent hidden geological structures that existed in the crust prior to the initiation of the DST fault. The complex shapes of these structures may be due to intensive tectonic processes in previous stages of geologic development of the region.

It is interesting that no prominent features are observed in the basin of the Gulf of Aqaba at all depth intervals, with the exception of the DST-aligned positive S-wave anomalies that are visible within an interval of 20-40 km and continue further north but are thought to be correlated with the DST rather than the Gulf of Aqaba itself. The lack of a prominent anomaly at shallow depths may indicate a relatively thin sedimentary covering, which does not considerably contribute to the seismic model, or insufficient resolution of our model at this depth. Compared with the shallow water basin of the Gulf of Suez, which is completely covered with sediments, the Gulf of Aqaba is deep and has strongly variable bathymetry features, which indicate that the rate of extension here exceeds the sedimentation rate. According to seismic surveys by Ben-Avraham et al. (1979), the maximum thickness of sediments in the Aqaba basin may reach 2-3 km, but the thickness appears to be strongly variable. The sedimentation in the Aqaba basin appears similar to the average sedimentary cover thickness in the surrounding onshore areas and thus does not produce a prominent relative negative anomaly in the shallow velocities. Furthermore, the ray configuration used in this study does not allow the recovery of shallow anomalies in the offshore areas.

In sections at depths of 20 and 30 km, we depict the markers of the lateral displacements since the initiation of the Dead Sea Fault with green dotted lines in Figure 7. The line along the coast, which has a step-shaped form after 100 km of left-lateral displacement, almost perfectly fits the transition between high- and low-velocity anomalies (Figure 10). This feature may indicate the deformation of the continental crust by the fault and corresponds well to the total estimates of the lateral displacements along the DST derived from independent sources.

At a 30 km depth, the negative anomaly along the Gulf of Aqaba (especially clear for the S-velocity model in Figure 7) possibly indicates crustal thinning and local heating due to the slip-parallel extension of the basin. However, seismic anomalies only indirectly represent crustal thickness variations, and they are sensitive to only large deviations of the Moho depth. Other methods, such as seismic reflection surveys or receiver function analysis, would be more suitable for this purpose.

At the 40 km depth, the structure corresponds with the uppermost mantle. As observed in synthetic tests, the vertical resolution of the S-model at this depth is poor. Therefore, this structure, which appears to similar to that at 30 km, is probably due to the vertical smearing and does not accurately represent distribution in the mantle. At the same time, the mantle structure for the P-velocity appears to be robust. The presence of high velocities in the uppermost mantle beneath the northern Red Sea at this depth does not confirm the hypothesis of significant hot asthenosphere upwelling, which would exist in the case of active rifting. This result supports the passive nature of extension, which is likely due to relative displacements of large lithospheric plates, namely the African and Arabian Plates.

At the 40 km depth, the structure of P-velocities is considerably different than that observed at the 30 km depth. Instead of the step-shaped contact zone identified at the 30 km depth, we observe a nearly linear transition oriented from SSE-NNW. This feature may represent the contrast between crustal velocities, which can still be observed at this depth for some segments of the thick crust, and mantle velocities in the remaining areas with thinner crust. According to the model of Moho depth from Mechie et al., (2013, Figure 5), this low-velocity anomaly at the 40 km depth corresponds to the area of the crust with a thickness of more than 35 km, which is thicker than the crust in surrounding areas.

It would be interesting to study the relative velocity anomalies at depths that fully correspond to the mantle to identify the link between mantle processes and crustal displacements. Unfortunately, our model does not have sufficient resolution for depths greater than 40 km. At our scale and in our area of interest, information on mantle structures can only be derived from analysis of teleseismic data. Such work was performed for the Dead Sea area by Koulakov et al., (2006), but it did not reveal any connection between crust and the mantle. If such a connection existed in the Aqaba region, however, it should be much clearer because both oceanic and continental mantle lithosphere coexist. Our future work will focus on analyzing the teleseismic records provided by stations distributed in the whole area and will provide rich information on mantle processes beneath the northern part of the Red Sea.

Conclusions

A large dataset containing arrival times from regional earthquakes provided by the Egyptian National Seismological Network was used for a tomographic investigation of the

Solid Earth Discuss., doi:10.5194/se-2016-2, 2016
Manuscript under review for journal Solid Earth
Published: 18 January 2016

crustal structure beneath the area of the Gulf of Aqaba and northern Red Sea. The main results of this work are the 3D models of P and S seismic velocities in the crust and uppermost mantle for these regions. These models close the gap between the existing small-scale active source studies of the uppermost crust beneath the offshore areas of the Red Sea and Gulf of Aqaba and large-scale regional mantle models beneath Africa and Arabia derived from the inversion of body and surface wave data.

The new seismic models reveal a strong high-velocity anomaly in the northern Red Sea, with sharp boundaries coinciding with the coastal line. This implies an oceanic type crust and seems to oppose the concept of gradual stretching of continental crust in the northern Red Sea proposed by some authors. However, the question about development of the oceanic crust, specifically regarding the absence of any traces of ridges and spreading centers in the northern Red Sea that would require a rather dispersed extension of oceanic crust opposed to spreading localized along rifts, still remains.

In the middle and lower crust, the seismic anomalies seem to delineate a step-shaped pattern, which indicates the left-lateral displacement of the crust along the Dead Sea Transform Fault. The estimated value of this displacement from the seismic tomography model is approximately 100 km; this is consistent with existing estimates from geological and geomorphology data for the southern part of the DST.

At the 40 km depth, no apparent link between the location of the Gulf of Aqaba and the DST fault zone is observed. Instead, there is a zone of relatively low P waves speed to the north of Aqaba continuously crossing the fault, which was also detected in the independent crustal model of Eastern Mediterranean by Koulakov and Sobolev (2006). It is not entirely clear how this continuous zone could be conserved after more than 100 km of displacement along the DST fault. Considering the relatively thin lithosphere (60-70 km), which has a tendency for southward thinning (Mohsen et al., 2006) in this region, one might assume that the anomalies are mostly controlled by present-day thermo-mechanical processes in the lower-most lithospheric mantle

Solid Earth Discuss., doi:10.5194/se-2016-2, 2016
Manuscript under review for journal Solid Earth
Published: 18 January 2016

and asthenosphere, rather than the tectonic history of the region. However, this question still requires further investigations.

Acknowledgments

Earthquake data of this study were obtained from the Egyptian National Seismological Network. IK is supported by the Russian Science Foundation (grant #14-17-00430). The authors extend their appreciation to the Deanship of Scientific Research at King Saud University for funding the work through the research group project RG -1435-027. AP is supported by German Research Foundation (DFG grant PE 2167/1-1).

Figure captions:

Figure 1. A. Major tectonic framework of the study area schematically representing the main displacements of the major plates. The blue line is the transform fault, the red lines are the divergent areas, and the violet line depict the convergent boundaries. DST is the Dead Sea Transform Fault. B. Tectonic units in the area of Gulf of Aqaba. Grey lines are faults in Egypt (Darwish and El Ababy, 1993, Bosworth and McClay, 2001); blue lines are the faults in Saudi Arabia and red dotted lines are dykes according to Eyal et al. (1981).

Figure 2. Back reconstruction of the displacements along the DST since the initiation in Early Miocene in the left (Eyal et al., 1981) and present topography along DST. Red lines mark the main structures at the initial stage for reference.

Figure 3. Distributions of seismic stations (blue triangles) and seismic events (orange dots) used in this study for tomographic inversion.

Figure 4. Distributions of the ray paths (grey dots) and nodes of the parameterization grid (red dots). Depth intervals and types of data are indicated in the caption.

Solid Earth Discuss., doi:10.5194/se-2016-2, 2016
Manuscript under review for journal Solid Earth
Published: 18 January 2016

Figure 5. Results of the checkerboard test with the model unchanged with depth for P and S velocity anomalies. Dotted lines indicate the configurations of the "true" synthetic patterns. Triangles depict seismic stations.

Figure 6. Checkerboard tests with the model changing the sign of anomalies at 20 km depth. Dotted lines indicate the configurations of the "true" synthetic patterns. Triangles depict seismic stations.

Figure 7. P and S anomalies resulted from the observed data inversion in four horizontal sections. At 10 km depth, major tectonic units, same as in Figure 1b, are shown. In sections at 20 and 30 km depth, the reference lines marking the displacements along the DST are depicted with green dotted lines.

Figure 8. Absolute P-velocity at 30 km depth and in four vertical sections. Locations of the sections are shown in the map. White dots are the projections of earthquakes onto the profiles.

Figure 9. Same as Figure 8, but for the S absolute velocities.

Figure 10. Back-reconstruction of the P-velocity model at 10 km and 30 km depth according to the DST displacements presented in Figure 2. Green dotted lines depict the reference markers for the displacement. Violet lines are the structures discussed in the text.

References

Abdel-Fattah, A. K., Hussein, H. M., Ibrahim, E. M., and El Atta, A. A.: Fault plane solutions of the 1993 and 1995 Gulf of Aqaba earthquakes and their tectonic implications, Annals of Geophysics, 40(6), 1997.

Bartov, Y., Steinitz G., Eyal M., and Eyal Y.: Sinistral movement along the Gulf of Aqaba—Its age and relation to the opening of the Red Sea, Nature, 285, 220–222, 1980.

Ben-Avraham, Z., Almagor, G., and Garfunkel, Z.: Sediments and structure of the Gulf of Elat (Aqaba) - northern Red Sea, Sedimentary Geology, 23(1), 239-267, 1979.

Solid Earth Discuss., doi:10.5194/se-2016-2, 2016
Manuscript under review for journal Solid Earth
Published: 18 January 2016

Ben-Avraham, Z.: Structural framework of the gulf of Elat (Aqaba), northern Red Sea, Journal of Geophysical Research: Solid Earth (1978–2012),90(B1), 703-726, 1985.

Ben-Avraham, Z and Zoback, M. D.: Transform-normal extension and asymmetric basins: An alternative to pull-apart models, Geology, 20(5), 423-426, 1992.

Bosworth, W., and McClay, K.: Structural and stratigraphic evolution of the Gulf of Suez rift, Egypt: a synthesis. Mémoires du Muséum national d'histoire naturelle, 186, 567-606, 2001.

Chang, S. J., and Van der Lee, S.: Mantle plumes and associated flow beneath Arabia and East Africa, Earth and Planetary Science Letters, 302(3), 448-454, 2011.

Chu, D., and Gordon, R. G.: Current plate motions across the Red Sea, Geophys. J. Int., 135, 313– 328, 1998.

Cochran J. R., and Martinez, F.: Evidence from the northern Red Sea on the transition from the continental to oceanic rifting, Tectonophysics 153, 25-53, 1988.

Cochran, J. R.: Northern Red Sea: Nucleation of an oceanic spreading center within a continental rift, Geochem. Geophys. Geosyst., 6, Q03006, doi:10.1029/2004GC000826, 2005.

Cochran, J. R., and Karner, G. D.: Constraints on the deformation and rupturing of continental lithosphere of the Red Sea: the transition from rifting to drifting, Geological Society, London, Special Publications 282.1, 265-289, 2007.

Darwish, M., and El Araby, A.: Petrography and diagenetic aspects of some siliciclastic hydrocarbon reservoirs in relation to rifting of the Gulf of Suez, Egypt. Geodynamics and sedimentation of the Red Sea-Gulf of Aden Rift System. Geologic Survey Egypt Special Publication, 1, 155-187, 1993.

DESERT Group: The crustal structure of the Dead Sea Transform, Geophys. J. Int., 156, 655 – 681, doi:10.1111/j.1365-246X.2004.02143.x, 2004.

Solid Earth Discuss., doi:10.5194/se-2016-2, 2016
Manuscript under review for journal Solid Earth
Published: 18 January 2016

Ehrhardt, A., Hubscher, C., Ben-Avraham, Z., and Gajewski, D.: Seismic study of pull-apart-induced sedimentation and deformation in the Northern Gulf of Aqaba (Elat), Tectonophysics, 396, 59–79, 2005.

Eyal, M., Eyal, Y., Bartov, Y., and Steinitz, G.: The tectonic development of the western margin of the Gulf of Elat (Aqaba) rift, Tectonophysics, 80(1), 39-66, 1981.

Freund, R., Zak, I., and Garfunkel, Z.: Age and rate of the sinistral movement along the Dead Sea rift, Nature, 220, 253–255, 1968.

Garfunkel, Z.: Internal structure of the Dead Sea leaky transform (rift) in relation to plate kinematics, Tectonophysics, 80, 81– 108, 1981.

Garfunkel, Z., Zak, I., and Freund, R.: Active faulting in the Dead Sea rift, Tectonophysics, 80, 1–26, 1981.

Gaulier, J. M., Le Pichon, X., Lyberis, N., Avedik, F., Geli, L., Moretti, I., Deschamps, A., and Hafez, S.: Seismic study of the crust of the northern Red Sea and Gulf of Suez, Tectonophysics, 153(1), 55-88, 1988.

Ginzburg, A., Makris, J., Fuchs, K., and Prodehl, C.: The structure of the crust and upper mantle in the Dead Sea rift, Tectonophysics, 80, 109–119, 1981.

Gomez, F., Karam, G., Khawlie, M., McClusky, S., Vernant, P., Reilinger, R., Jaafar, R., Tabet, C., Khair, K., and Barazangi, M.: Global Positioning System measurements of strain accumulation and slip transfer through the restraining bend along the Dead Sea fault system in Lebanon. Geophysical Journal International, 168(3), 1021-1028, 2007.

Hartman, G., Niemi, T. M., Tibor, G., Ben-Avraham, Z., Al-Zoubi, A., Makovsky, Y., Akawwi, E., Abueladas, A.-R., and Al-Ruzouq, R.: Quaternary tectonic evolution of the Northern Gulf of Elat/Aqaba along the Dead Sea Transform, Journal of Geophysical Research: Solid Earth, 119 (12) 9183-9205, DOI: 10.1002/2013JB010879, 2014.

Hofstetter, A.: Seismic observations of the 22/11/1995 Gulf of Aqaba earthquake sequence, Tectonophysics, 369(1), 21-36, 2003.

Solid Earth Discuss., doi:10.5194/se-2016-2, 2016
Manuscript under review for journal Solid Earth
Published: 18 January 2016

Joffe, S., and Garfunkel, Z.:, Plate Kinematics of the circum Red Sea—a re-evaluation, Tectonophysics, 141, 5 – 22, 1987.

Khrepy, S., Koulakov, I., Al-Arifi, N.: Crustal structure beneath the continental rifting area of Gulf of Suez from earthquakes tomography, Tectonophysics, accepted, 2016.

Koulakov, I.: LOTOS code for local earthquake tomographic inversion. Benchmarks for testing tomographic algorithms, Bulletin of the Seismological Society of America, Vol. 99, No. 1, pp. 194-214, doi: 10.1785/0120080013, 2009.

Koulakov, I., and Sobolev, S. V.: Moho depth and three-dimensional P and S structure of the crust and uppermost mantle in the Eastern Mediterranean and Middle East derived from tomograpic inversion of local ISC data, Geophysical Journal International, 164, 1, 218-235, 2006.

Koulakov, I., Sobolev, S.V., Weber, M., Oreshin, S., Wylegalla, K., and Hofstetter, R.: Teleseismic tomography reveals no signature of the Dead Sea Transform in the upper mantle structure, Earth and Planetary Science Letters. 252, 1-2, 189-200, 2006.

Koulakov, I., Burov E., Cloetingh, S., El Khrepy, S., Al-Arifi, N., and Bushenkova N.: Evidences for a plume beneath the Arabian Platform from travel time tomography inversion, Tectonophysics, accepted, 2016.

Mahmoud, S., Reilinger, R., McClusky, S., Vernant, P., and Tealeb, A.: GPS evidence for northward motion of the Sinai Block: Implications for E. Mediterranean tectonics, Earth and Planetary Science Letters, 238(1), 217-224, 2005.

Makovsky, Y., Wunch, A., Ariely, R., Shaked, Y., Rivlin, A., Shemesh, A., Ben Avraham, Z., and Agnon, A.: Quaternary transform kinematics constrained by sequence stratigraphy and submerged coastline features, The Gulf of Aqaba, Earth Planet. Sci. Lett., 271, 109–122, 2008.

Mann, P., Hempton, M. R., Bradley, D. C., and Burke, K.: Development of pull-apart basins, The Journal of Geology, 529-554, 1983.

Solid Earth Discuss., doi:10.5194/se-2016-2, 2016
Manuscript under review for journal Solid Earth
Published: 18 January 2016

McClusky, S., Reilinger, R., Mahmoud, S., Ben Sari, D., and Tealeb, A.: GPS constraints on Africa (Nubia) and Arabia plate motions, Geophys. J. Int., 155, 126– 138, 2003.

McKenzie, D. P., Davies, D., and Molnar, P.: Plate tectonics of the Red Sea and East Africa, Nature, 226, 243-248, 1970.

Mechie, J., Abu-Ayyash, K., Ben-Avraham, Z., El-Kelani, R., Mohsen, A., Rumpker, G., Saul, J., and Weber, M.: Crustal shear velocity structure across the Dead Sea Transform from twodimensional modelling of DESERT project explosion seismic data, Geophys. J. Int., 160, 910–924, doi:10.1111/j.1365-246X.2005.02526.x, 2005.

Mechie, J., Ben-Avraham, Z., Weber, M., Götze, H.-J., Koulakov, I., Mohsen, A., and Stiller, M.: The distribution of Moho depths beneath the Arabian plate and margins, Tectonophysics, 609, 234-249, doi:10.1016/j.tecto.2012.11.015, 2013.

Mohsen, A., Kind, R., Sobolev, S. V., Weber, M., and the DESERT Group: Thickness of the lithosphere east of the Dead Sea Transform, Geophys. J. Int., 167, 845–852, doi:10.1111/j.1365-246X.2006.03185.x, 2006.

Nolet, G.: Seismic wave propagation and seismic tomography, in: Seismic tomography, Springer, pp. 1-23, 1987.

Paige, C. C., and Saunders, M. A.: LSQR: An algorithm for sparse linear equations and sparse least squares, ACM Transactions on Mathematical Software (TOMS). 8, 43-71, 1982.

Park, Y., Nyblade A. A., Rodgers, A. J., and Al Amri, A.: S wave velocity structure of the Arabian Shield upper mantle from Rayleigh wave tomography, Geochem, Geophys. Geosyst., 9, Q07020, doi:10.1029/2007GC001895, 2008.

Petrunin, A. G., and Sobolev, S. V.: Three-dimensional numerical models of the evolution of pull-apart basins, Phys. Earth Planet. Inter., 171(1-4), 387–399, doi:10.1016/j.pepi.2008.08.017, 2008.

Solid Earth Discuss., doi:10.5194/se-2016-2, 2016
Manuscript under review for journal Solid Earth
Published: 18 January 2016

Petrunin, A. G., Meneses Rioseco, E., Sobolev, S. V., and Weber, M.: Thermomechanical model reconciles contradictory geophysical observations at the Dead Sea Basin, Geochemistry Geophys. Geosystems, 13, doi:10.1029/2011GC003929, 2012.

Ritter, O., Ryberg, T., Weckmann, U., Hoffmann-Rothe, A., Abueladas, A., Garfunkel, Z., and DESERT Research Group: Geophysical images of the Dead Sea Transform in Jordan reveal an impermeable barrier for fluid flow, Geophys. Res. Lett., 30(14), 1741, doi:10.1029/2003GL017541, 2003.

Smit, J., Brun, J.-P., Cloetingh, S., and Ben-Avraham, Z.: The rift-like structure and asymmetry of the Dead Sea Fault, Earth Planet. Sci. Lett., 290(1-2), 74–82, doi:10.1016/j.epsl.2009.11.060, 2010.

Smith, D. E., Kolenkiewicz, R., Robbins, J. W., Dunn, P. J., and Torrence, M. H.: Horizontal crustal motion in the central and eastern Mediterranean inferred from satellite laser ranging measurements, Geophys. Res. Lett., 21, 1979– 1982, 1994.

Ten Brink, U. S., Ben-Avraham, Z., Bell, R. E., Hassouneh, M., Coleman, D. F., Andreasen, G., and Coakley, B.: Structure of the Dead Sea pull‐apart basin from gravity analyses, Journal of Geophysical Research: Solid Earth (1978–2012), 98(B12), 21877-21894, 1993.

Um, J., and Thurber, C. H.: A fast algorithm for two-point seismic ray tracing, Bull. Seism. Soc. Am., 77, 972-986, 1987.

Wdowinski, S., Bock, Y., Baer, G., Prawirodirdjo, L., Bechor, N., Naaman, S., Knafo, R., Forrai, Y., and Melzer, Y.: GPS measurements of current crustal movements along the Dead Sea Fault, J. Geophys. Res., 109, B05403, doi:10.1029/2003JB002640, 2004.

Weber, M., Abu-Ayyash, K., Abueladas, A., Agnon, A., Tasarova, Z., Al-Zubi, H., Babeyko, A., Bartov, Y., Bauer, K., Becken, M., Bedrosian, P. A., Ben-Avraham, Z., Bock, G., Bohnhoff, M., Bribach, J., Dulski, P., Ebbing, J., El-Kelani, R., Forster, A., Forster, H.J., Frieslander, U., Garfunkel, Z., Goetze, H. J., Haak, H., Haberland, C., Hassouneh,

Solid Earth Discuss., doi:10.5194/se-2016-2, 2016
Manuscript under review for journal Solid Earth
Published: 18 January 2016

M., Helwig, S., Hofstetter, A., Hoffmann-Rothe, A., Jaeckel, K.H., Janssen, C., Jaser, D., Kesten, D., Khatib, M., Kind, R., Koch, O., Koulakov, I., Laske, G., Maercklin, N., Masarweh, R., Masri, A., Matar, A., Mechie, J., Meqbel, N., Plessen, B., Moeller, P., Mohsen, A., Oberhansli, R., Oreshin, S., Petrunin, A., Qabbani, I., Rabba, I., Ritter, O., Romer, R., Rumpker, G., Rybakov, M., Ryberg, T., Saul, J., Scherbaum, F., Schmidt, S., Schulze, A., Sobolev, S.V., Stiller, M., Stromeyer, D., Tarawneh, K., Trela, C., Weckmann, U., Wetzel, H.-U., and Wylegaala, K.: Anatomy of the Dead Sea Transform from lithospheric to microscopic scale, Rev. Geophys., 47, RG2002, doi:10.1029/2008RG000264, 2009.

Solid Earth Discuss., doi:10.5194/se-2016-2, 2016
Manuscript under review for journal Solid Earth
Published: 18 January 2016

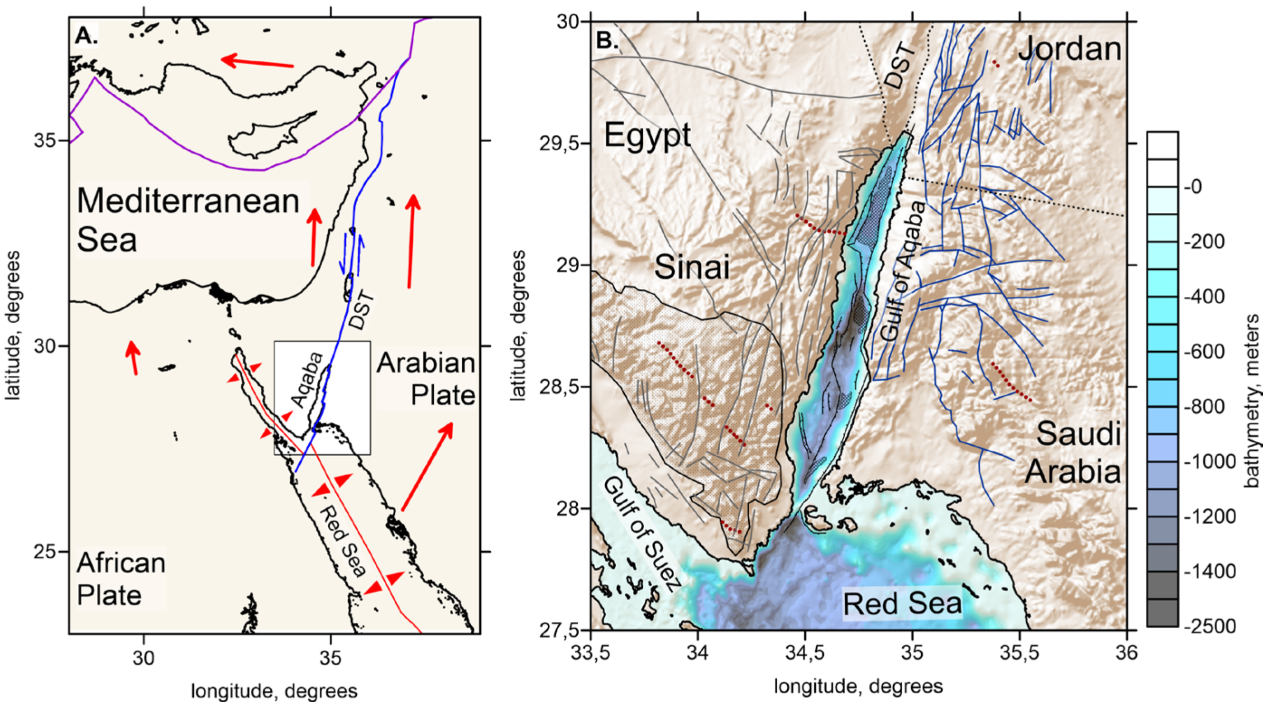

Figure 1. A. Major tectonic framework of the study area schematically representing the main displacements of the major plates. The blue line is the transform fault, the red lines are the divergent areas, and the violet line depict the convergent boundaries. DST is the Dead Sea Transform Fault. B. Tectonic units in the area of Gulf of Aqaba. Grey lines are faults in Egypt [*Darwish and El Ababy,* 1993, *Bosworth and McClay,* 2001]; blue lines are the faults in Saudi Arabia and red dotted lines are dykes according to *Eyal et al.* [1981].

Solid Earth Discuss., doi:10.5194/se-2016-2, 2016
Manuscript under review for journal Solid Earth
Published: 18 January 2016

Solid Earth
Discussions
Open Access

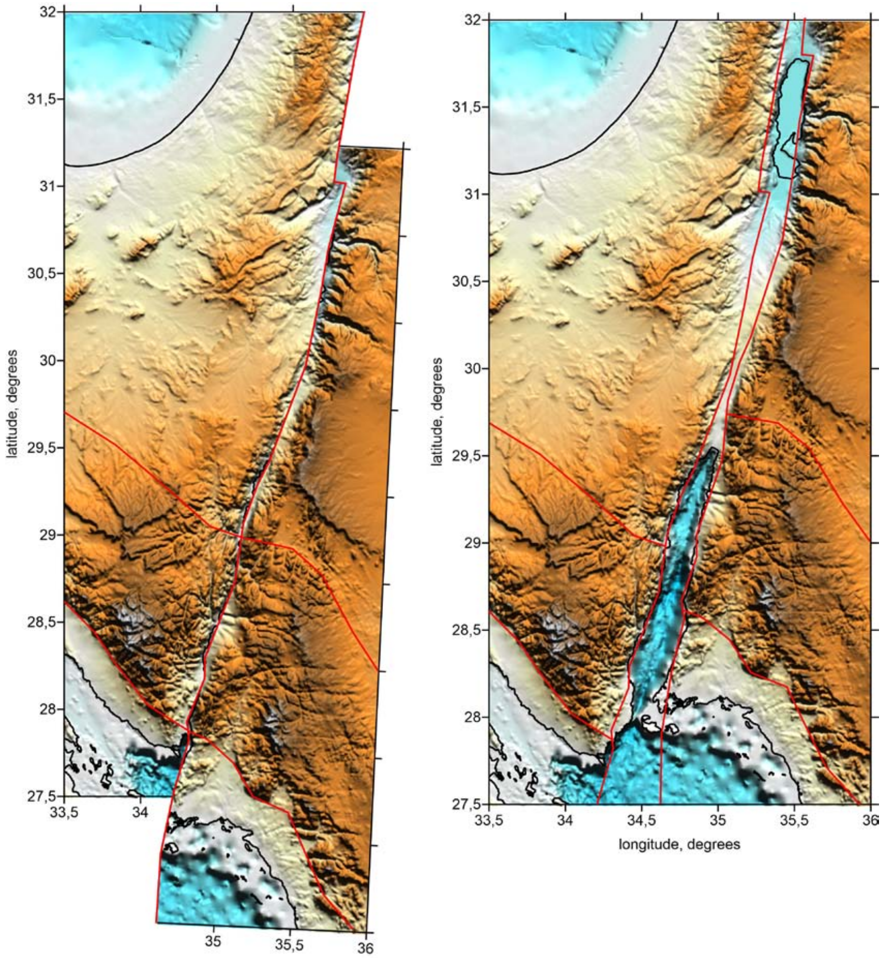

Figure 2. Back reconstruction of the displacements along the DST since the initiation in Early Miocene in the left [*Eyal et al.,* 1981] and present topography along DST. Red lines mark the main structures at the initial stage for reference.

Solid Earth Discuss., doi:10.5194/se-2016-2, 2016
Manuscript under review for journal Solid Earth
Published: 18 January 2016

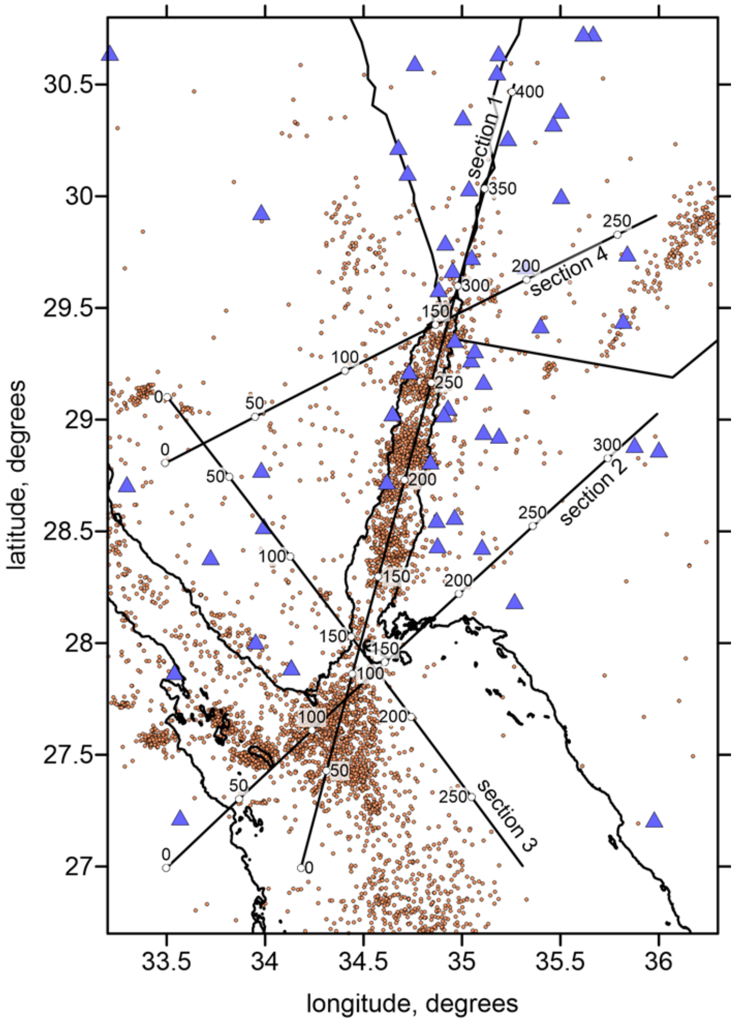

Figure 3. Distributions of seismic stations (blue triangles) and seismic events (orange dots) used in this study for tomographic inversion.

Solid Earth Discuss., doi:10.5194/se-2016-2, 2016
Manuscript under review for journal Solid Earth
Published: 18 January 2016

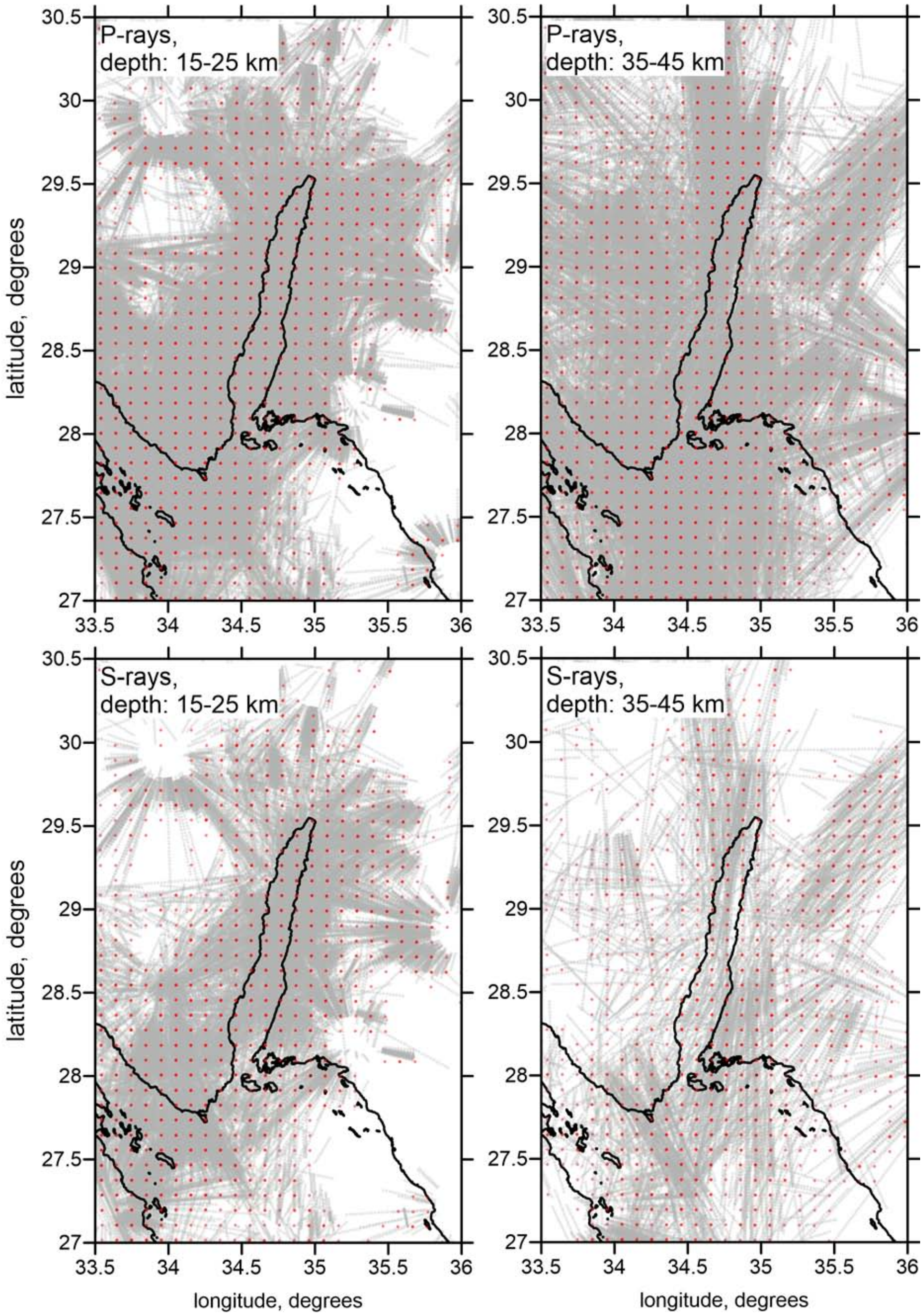

Figure 4. Distributions of the ray paths (grey dots) and nodes of the parameterization grid (red dots). Depth intervals and types of data are indicated in the caption.

Solid Earth Discuss., doi:10.5194/se-2016-2, 2016
Manuscript under review for journal Solid Earth
Published: 18 January 2016

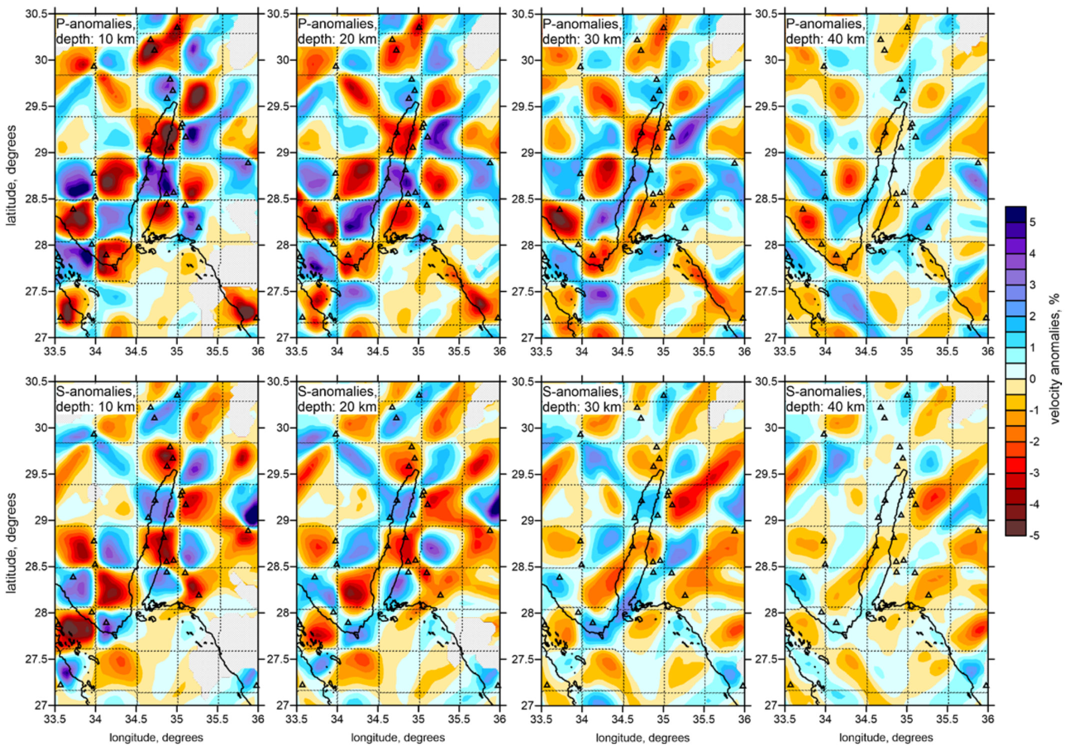

Figure 5. Results of the checkerboard test with the model unchanged with depth for P and S velocity anomalies. Dotted lines indicate the configurations of the "true" synthetic patterns. Triangles depict seismic stations.

Solid Earth Discuss., doi:10.5194/se-2016-2, 2016
Manuscript under review for journal Solid Earth
Published: 18 January 2016

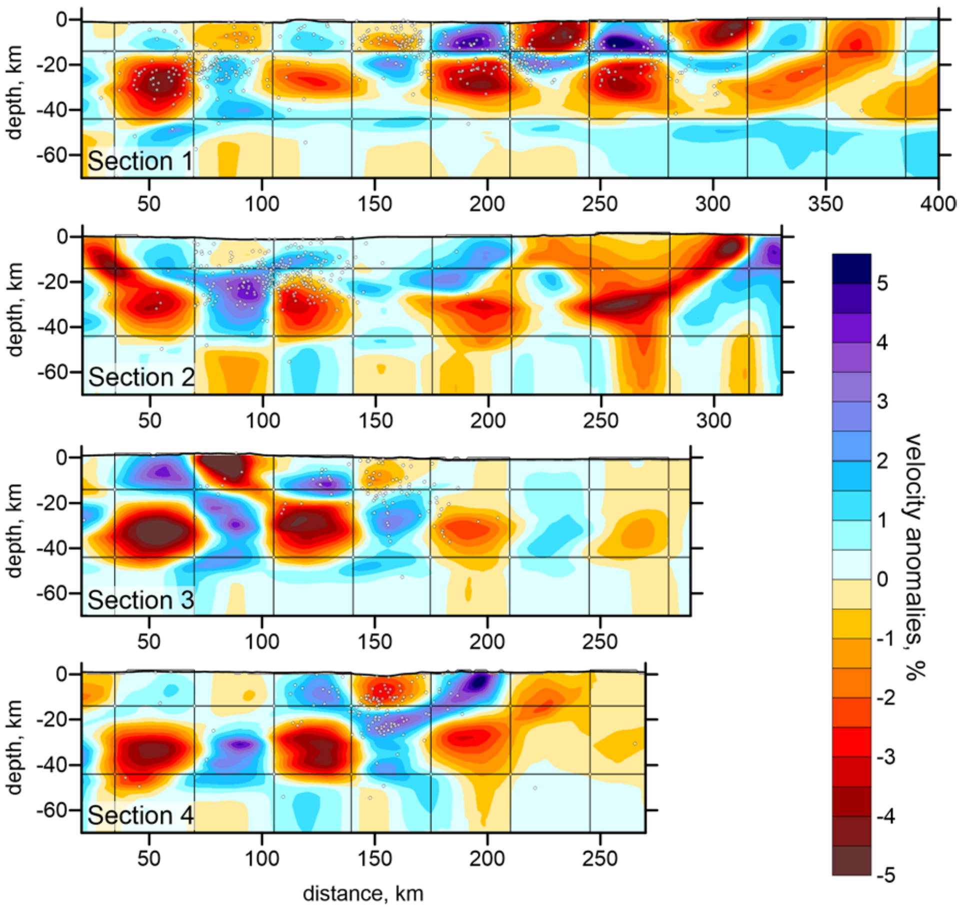

Figure 6. Checkerboard tests with the model changing the sign of anomalies at 20 km depth. Dotted lines indicate the configurations of the “true” synthetic patterns. Triangles depict seismic stations.

Solid Earth Discuss., doi:10.5194/se-2016-2, 2016
Manuscript under review for journal Solid Earth
Published: 18 January 2016

Solid Earth
Discussions
Open Access

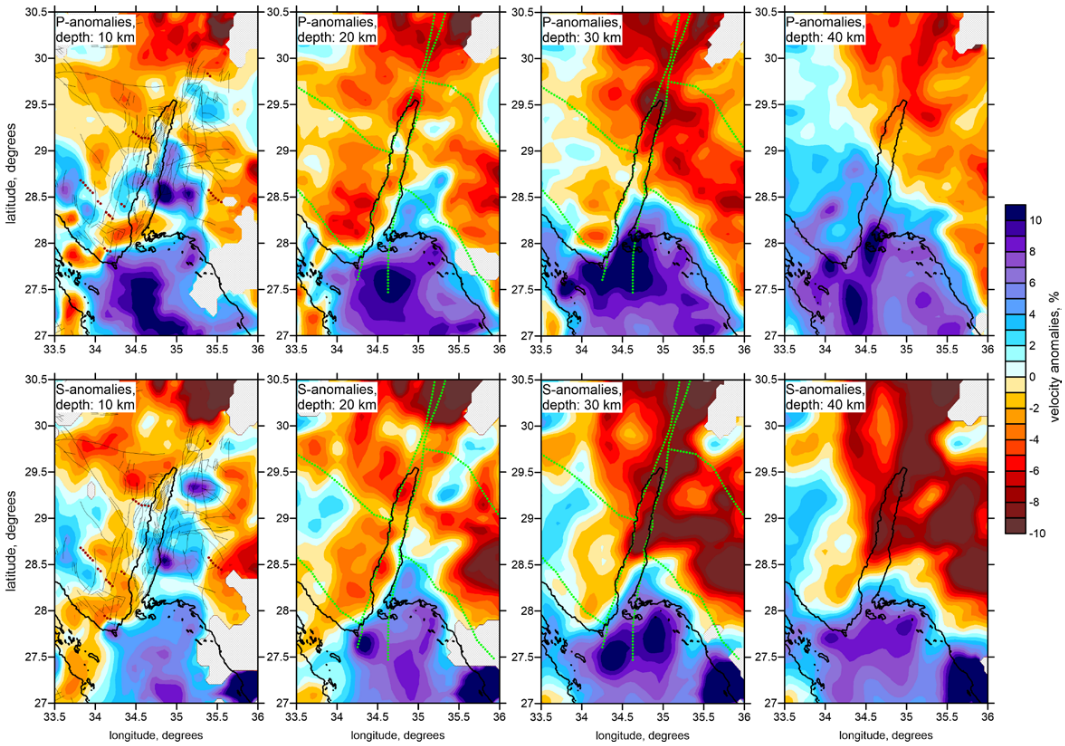

Figure 7. P and S anomalies resulted from the observed data inversion in four horizontal sections. At 10 km depth, major tectonic units, same as in Figure 1b, are shown. In sections at 20 and 30 km depth, the reference lines marking the displacements along the DST are depicted with green dotted lines.

Solid Earth Discuss., doi:10.5194/se-2016-2, 2016
Manuscript under review for journal Solid Earth
Published: 18 January 2016

Solid Earth
Discussions
Open Access

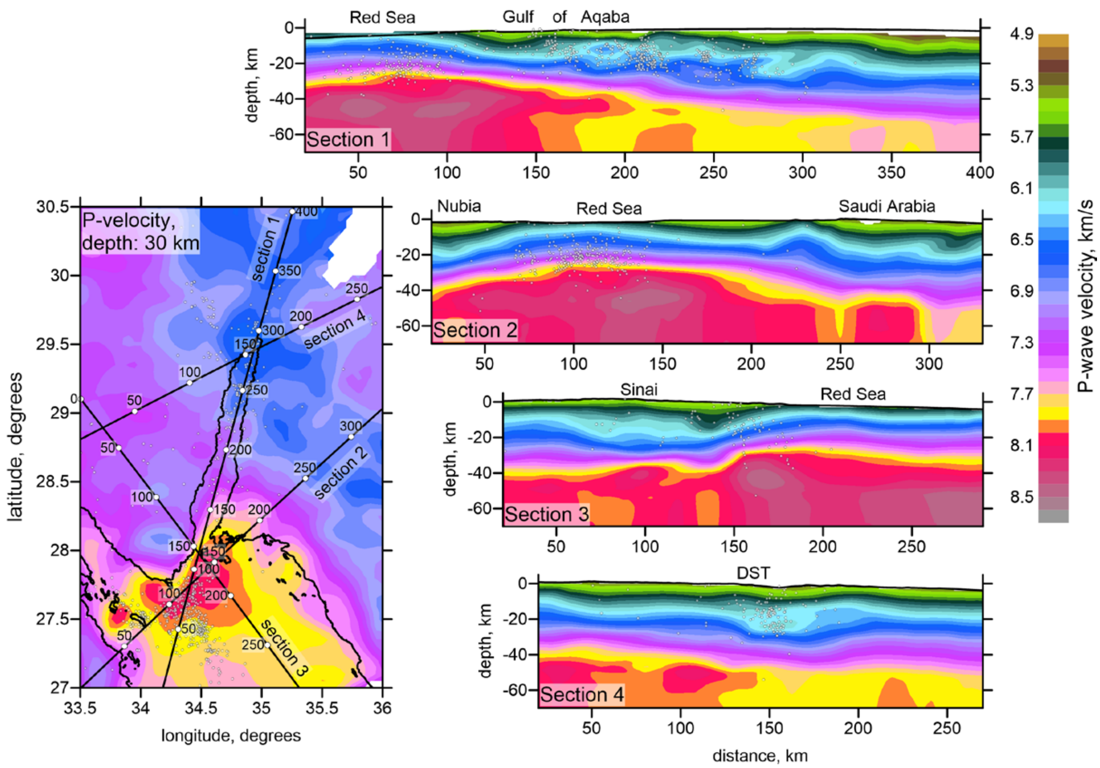

Figure 8. Absolute P-velocity at 30 km depth and in four vertical sections. Locations of the sections are shown in the map. White dots are the projections of earthquakes onto the profiles.

Solid Earth Discuss., doi:10.5194/se-2016-2, 2016
Manuscript under review for journal Solid Earth
Published: 18 January 2016

Solid Earth
Discussions

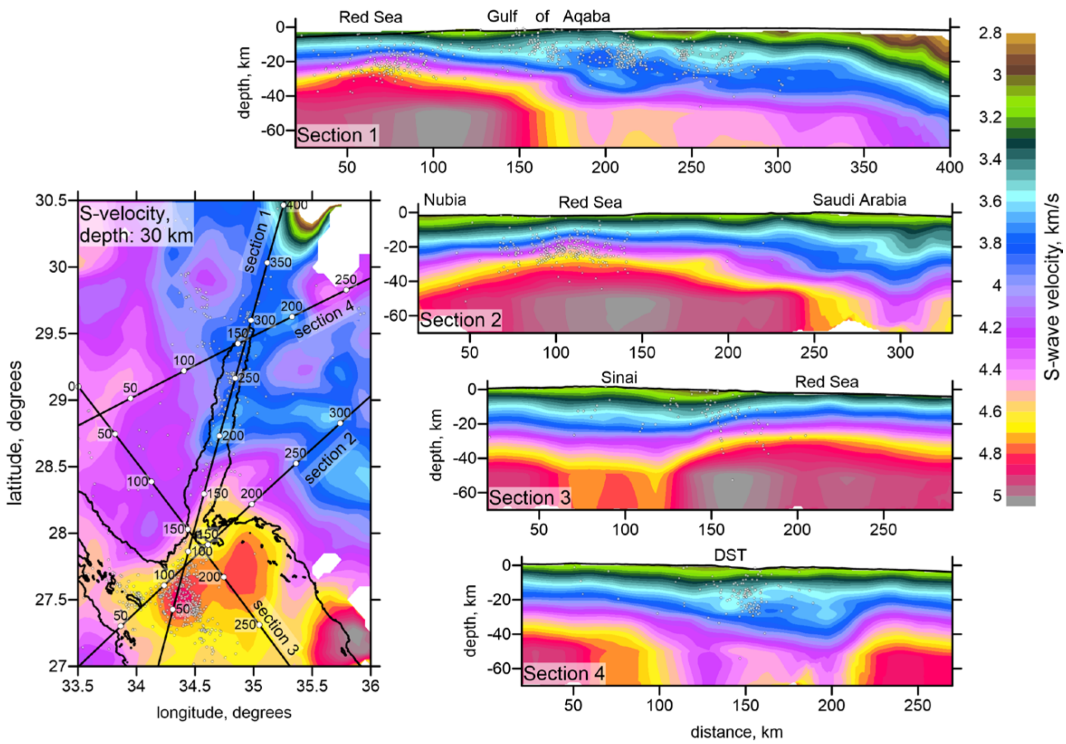

Figure 9. Same as Figure 8, but for the S absolute velocities.

Solid Earth Discuss., doi:10.5194/se-2016-2, 2016
Manuscript under review for journal Solid Earth
Published: 18 January 2016

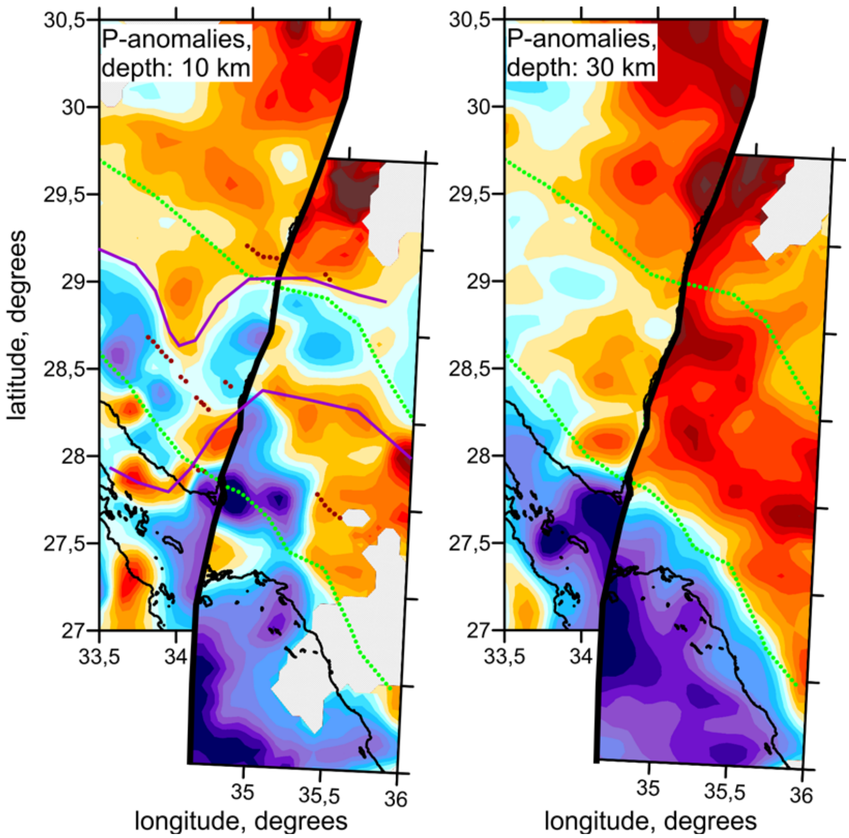

Figure 10. Back-reconstruction of the P-velocity model at 10 km and 30 km depth according to the DST displacements presented in Figure 2. Green dotted lines depict the reference markers for the displacement. Violet lines are the structures discussed in the text.